Particle Accelerators, 1993, Vol. 43(1–2), pp. 93–105
Reprints available directly from the publisher
Photocopying permitted by license only

REALIZATION OF IMPROVED EFFICIENCY IN A GYROKLYSTRON AMPLIFIER*

G. S. PARK, P. M. MALOUF, and V. L. GRANATSTEIN†

Omega-P, Inc., 2008 Yale Station, New Haven, CT 06520

C. M. ARMSTRONG and A. K. GANGULY

Naval Research Laboratory, Washington, DC 20375

(Received 4 January 1993; in final form 2 August 1993)

Gyroklystron amplifiers are being evaluated as possible microwave driver tubes for future TeV linear colliders. While gyroklystron power level and frequency capabilities look very promising, there is concern that amplifier efficiency has been only ~30%. In the present paper, we describe a gyroklystron amplifier study in which the pitch angle was large ($\alpha = v_\perp / v_z = 2$) and the efficiency was 40%. The amplifier voltage was relatively modest (45 kV), and there is reason to believe that still larger efficiency might be realized in higher voltage gyroklystrons. The theoretical basis for simulating gyrotron operation in the nonlinear regime is presented, and efficiency calculations are shown to be in good agreement with the experiment.

KEY WORDS: Electron beam devices, power supplies, radio-frequency devices

1 INTRODUCTION

Gyroklystrons are microwave amplifiers in which an input signal bunches electrons in phase in their cyclotron orbits, and coherent cyclotron emission produces an amplified microwave signal in an output cavity. In contrast to conventional klystrons, gyroklystrons require no small gaps in the cavities and have been successfully operated with higher – order transverse cavity modes and relatively large diameter drift spaces that are not cut off for lower order modes. Because of the absence of small gaps in which breakdown might occur, and because of their larger cross-sectional dimensions, gyroklystrons promise to be capable of performance exceeding more conventional microwave amplifiers especially when higher power and shorter wavelengths than the current state-of-the-art are desired. For this reason, gyroklystrons are being evaluated for such applications as driving TeV-class linear colliders. An important consideration in this application is microwave amplifier efficiency, since average power consumption

* Supported in part by the Office of Naval Technology

† Permanent address: University of Maryland, College Park, MD 20742

by the collider system would become prohibitive if the microwave amplifiers were inefficient.

Early gyroklystron studies at Varian Associates in the 1970's[1] achieved an efficiency of 10%. Since then, much progress has been made in understanding and optimizing gyroklystron performance. A high-power gyroklystron experiment at the University of Maryland[2] in 1991–1992 yielded output power of 29 MW at 9.85 GHz with 33% efficiency; a recent extension of this work[3] in which the output cavity was tuned to twice the input frequency yielded 30-MW output pulses at 19.7 GHz with 27% efficiency. In these studies the amplifier tube voltage was in the range 425–440 kV and the pulse duration was $\sim 1\mu$s. While these initial results are very encouraging and, in important respects, already surpass the best performance of conventional klystrons, the achieved efficiency falls short of the 50% level that is usually assumed in collider designs.[4]

Gyroklystrons consist of a temperature-limited magnetron injection gun and a number of resonant cavities separated by drift spaces, as shown in Figure 1. A hollow beam of spiraling electrons is injected into the amplifier circuit consisting of the cavities and drift spaces A salient parameter of the spiraling electrons is their pitch angle, $\alpha = v_\perp / v_z$. Too high a value of pitch angle results in instability. On the other hand, since gyrotrons primarily convert transverse electron energy into microwave radiation, a low value of pitch angle will limit amplifier efficiency. In the University of Maryland gyroklystron experiment[2] mentioned above, 33% efficiency was achieved with a relatively low value of pitch angle, $\alpha = v_\perp / v_z = 0.8$; thus, transverse efficiency was close to 80%. It seems clear that if gyroklystrons could be made to operate with reasonable stability at higher values of pitch angle, output efficiency might be significantly improved.

This paper describes an experimental study of a gyrotron with relatively modest values of frequency (4.5 GHz) and output power (< 100 kW). However, the pitch angle was $\alpha = 2$, large compared with the University of Maryland gyroklystron. This 4.5-GHz gyroklystron had originally been designed to operate with a uniform magnetic field, three resonantly tuned cavities, and a voltage of 60 kV; the design study had predicted output efficiency of 40%.[5] However, previous experimental studies of this amplifier had been limited to operating voltages of 35 kV, and although a concerted effort was made to optimize efficiency by shaping the magnetic field strength along the axis and by penultimate cavity detuning, the best obtainable output efficiency at the derated voltage was only 30%.[6] In the present experiment described below, the intention was to operate the gyroklystron at higher voltage (closer to the original design value) and to realize larger output efficiency.

2 DESCRIPTION OF THE EXPERIMENT

The three-cavity gyroklystron experiment is shown in Figure 1. All three rectangular cavities operate in the TE_{101} mode and are tunable by mechanically moving a narrow side wall in and out. The entire circuit is immersed in a solenoidal magnetic field adjusted to a value that brings the electron cyclotron frequency close to the

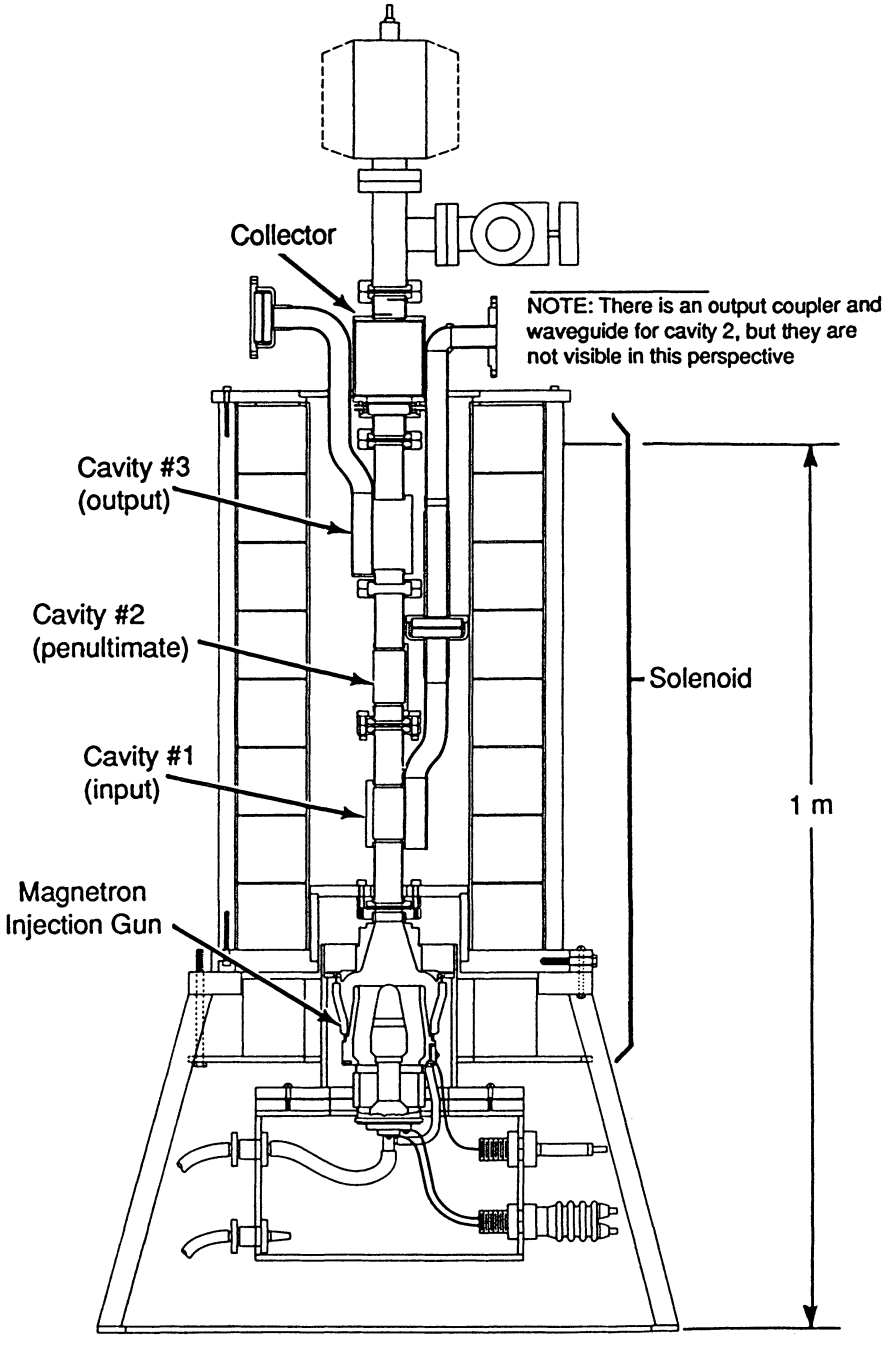

FIGURE 1: Three-cavity gyroklystron experimental configuration.

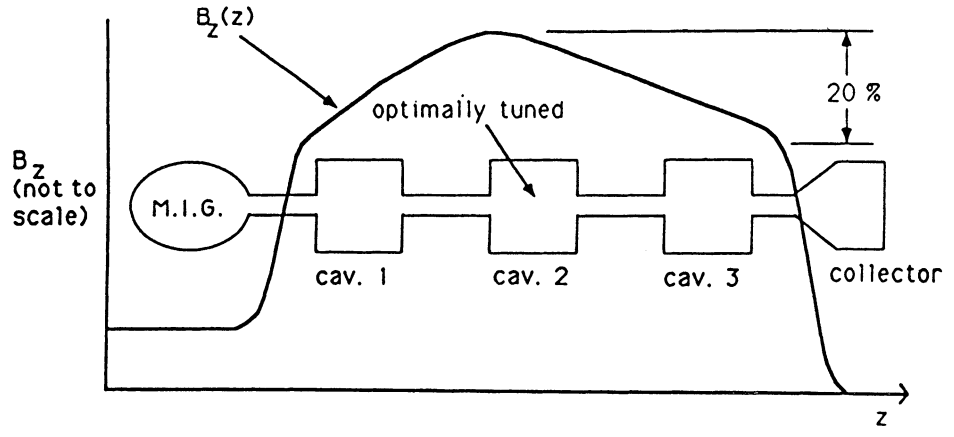

FIGURE 2: Profile of applied magnetic field along axis of gyroklystron circuit.

signal frequency. The electron energy is modulated by the rf signal in the input cavity. The cyclotron frequencies, which are dependent on the electrons' energies, then vary, and the electrons become bunched in phase in their cyclotron orbits as they pass through the drift spaces and cavity number two. The phase bunching may be optimized by detuning this penultimate cavity to a resonant frequency below the signal frequency.

In the output cavity, the phase-bunched electrons coherently radiate at the electron cyclotron frequency. This process converts a large fraction of the electron transverse energy into microwave output energy. Shaping the externally applied magnetic field along the circuit axis as shown in Figure 2 was found to optimize output power and efficiency.

3 NONLINEAR SIMULATION

A nonlinear analysis has been developed to model and optimize the design parameters for the operation of a multi-cavity gyroklystron amplifier. The analysis is based on a slow-time-scale formulation[7–10] in three dimensions developed for the steady-state operation of gyrotron traveling wave amplifiers. The set of coupled nonlinear gyrotron equations derived for the amplifiers may be used to describe the saturation properties of the oscillators by applying appropriate boundary conditions to the axial profile function of the rf field components. In this formulation, the electromagnetic field is expanded as a superposition of the unperturbed TE and TM modes of an empty waveguide. By averaging Maxwell's equations over a wave period, a series of slow-time-scale equations is derived for the evolution of the amplitude and phase of each TE and TM mode as driven by an electron beam in an applied guide magnetic field.

In general, the guide magnetic field is axisymmetric but nonuniform. The modes are coupled through their mutual nonlinear interactions with the ensemble of beam electrons. The wave-period averaging allows multi-mode interactions to be considered, provided that the frequencies are integral multiples of a fundamental frequency, and that the time average is done over the fundamental wave period. In this case, the particles that enter the interaction region at times to separated by integral multiples of the fundamental wave period will execute identical trajectories even though they interact with many modes. The time-averaged field equations are then integrated simultaneously with the three-dimensional Lorentz-force equations. No averaging is done for the orbit equations. The trajectory of each particle is calculated by summing contributions from each mode.

The nonlinear gyrotron equations, including the effects of guiding-center motion, axial velocity spread of electrons, and nonuniform guide field, have been derived in References 7 and 8 for rectangular electrodynamic structures and in References 9 and 10 for the cylindrical geometry. To model the experiment, we consider the excitation of only a single mode in this paper. The relevant equations for operation with the rectangular TE_{101} mode in the fundamental cyclotron harmonic are shown below.

The RF electric and magnetic field components of the TE_{101} mode in the rectangular cavity may be written as

$$\begin{aligned} E_y &= \sqrt{2/L_x L_y}\,\sin(k_t x)\,F(z)\,e^{i\omega t}\,, \\ B_x &= -\frac{i}{\omega}\sqrt{2/L_x L_y}\,\sin(k_t x)\,\frac{\partial F(z)}{\partial Z}e^{i\omega t}\,, \\ B_z &= \frac{i\pi}{\omega L_x}\sqrt{2/L_x L_y}\,\cos(k_t x)\,F(z)\,e^{i\omega t}\,, \end{aligned} \tag{1}$$

where L_x and L_y ($< Lx$) are the transverse dimensions of the cavity, $k_t = \pi/L_x$ is the transverse wave vector, and ω is the angular frequency of the wave. The axial (z-axis) dependence of the field in the cavity is given by the complex profile function

$$F(z) = F_R + iF_I = A(z)\,e^{-i\xi}\,. \tag{2}$$

$F(z)$ should satisfy proper boundary conditions at the two ends of the cavity. The amplitude A and the derivative $d\xi/dz$ are assumed to vary slowly in space.

The dynamical equations that govern the evolution of the amplitude (A) and phase (ξ) of a TE_{101} mode were derived in Reference 7 and are repeated here for convenience. The dispersion of the mode in the presence of the electron beam is given by

$$\frac{d^2A}{dz^2} + \left(\frac{\omega^2}{c^2} - k_t^2 - \left(\frac{d\xi}{dz}\right)^2\right)A = -2I\mu\omega\sum_{s=-\infty}^{\infty}\left\langle \frac{v_{z0}}{\langle v_{z0}\rangle}\,\frac{v_\perp}{|v_z|}\,N_1\,J_1'(k_t r_L)\,\sin\bar{\theta}\right\rangle\,, \tag{3}$$

and the growth of the mode is given by

$$\frac{d}{dz}\left(\frac{d\xi}{dz}\,A^2\right) = -2I\mu\omega A\sum_{s=-\infty}^{\infty}\left\langle \frac{v_{z0}}{\langle v_{z0}\rangle}\,\frac{v_\perp}{|v_z|}\,N_1\,J_1'(k_t r_L)\,\cos\bar{\theta}\right\rangle\,, \tag{4}$$

where $N_1 = \sqrt{2/L_x L_y}\,\sin k_t X_0$, the detuning parameter $\bar{\theta} = \omega t - \xi - \Psi$, and Ψ is the phase of the electrons. J_1 and J_1' are, respectively, the regular Bessel function of order one, and its derivative. I is the electron beam current. The axial and the perpendicular velocity components of an electron are denoted by v_z and $v_\perp$, respectively. The axial velocity of the electrons at the entrance to the cavity is denoted by v_{z0}. The guiding center coordinates of the electrons are X_0 and Y_0, and $r_L = \gamma v_\perp/\Omega_0$ is the Larmor radius. The relativistic factor is $\gamma = 1/\sqrt{1-(v_\perp^2+v_z^2)/c^2}$ and the cyclotron frequency is $\Omega_0 = eB_0(z)/m_0$. μ is the vacuum permittivity. The angle brackets denote an average over the initial phase-space distribution of the electrons. Conductive losses in the walls of the cavity may be approximately included in the calculations by replacing ω^2 in the dispersion relation, Equation (3), with $\omega^2(1-1/Q_c)$ and adding a term $\omega^2 A/c^2 Q_c$ on the left-hand side of the growth equation, Equation (4). Q_c is the quality factor of a cavity due to wall losses.

The electron orbit equations must also be specified to complete the formulation. The variation of electron momentum and phase are given by[7]

$$\frac{du_\perp}{dz} = \frac{1}{2}\frac{\partial\Omega_0}{\partial z} r_L - \frac{eAN_1}{m_0 v_z} J_1'(k_t r_L)\left\{\left(1 - \frac{v_z}{\omega}\frac{\partial\xi}{\partial z}\right)\cos\bar{\theta} + \frac{\Gamma v_z}{\omega}\sin\bar{\theta}\right\},$$

$$\frac{du_z}{dz} = -\frac{1}{2}\frac{\partial\Omega_0}{\partial z}\alpha r_L - \frac{eAN_1\alpha}{m_0\omega} J_1'(k_t r_L)\left\{\frac{\partial\xi}{\partial z}\cos\bar{\theta} - \Gamma\sin\bar{\theta}\right\}, \tag{5}$$

$$\frac{d\Psi}{dz} = \frac{\partial\Omega_0}{\gamma v_z} - \frac{eAN_1}{\gamma m_0 v_z v_\perp}\frac{J_1(k_t r_L)}{k_t r_L}\left\{\left(1 - \frac{v_z}{\omega}\frac{\partial\xi}{\partial z} - \frac{k_t^2 r_L^2 \Omega_0}{\gamma\omega}\right)\sin\bar{\theta} - \frac{\Gamma v_z}{\omega}\cos\bar{\theta}\right\},$$

where $u_\perp = \gamma v_\perp$, $u_z = \gamma v_z$, $\alpha = v_\perp/v_z$, $N_2 = \sqrt{2/L_x L_y}\,\cos k_t X_0$, and $\Gamma = \frac{1}{A}\frac{dA}{dz}$ is the growth rate of the amplitude.

The equations for the guiding-center motion may be written as

$$\frac{dX_0}{dz} = -\frac{1}{2\Omega_0}\frac{\partial\Omega_0}{\partial z} X_0 + \frac{eAN_2}{m_0 v_z \Omega_0} J_1(k_t r_L)\left\{\left(1 - \frac{v_z}{\omega}\frac{\partial\xi}{\partial z} - \frac{\Omega_0}{\gamma\omega}\right)\cos\bar{\theta} + \frac{\Gamma v_z}{\omega}\sin\bar{\theta}\right\},$$

$$\frac{dY_0}{dz} = -\frac{1}{2\Omega_0}\frac{\partial\Omega_0}{\partial z} Y_0 + \frac{eAN_2}{m_0\gamma v_z}\frac{k_t r_L}{\omega} J_1'(k_t r_L)\sin\bar{\theta}\,. \tag{6}$$

The transmitted power in the mode is calculated from the Poynting flux. The time-averaged power flow is given by

$$P = \frac{1}{2\mu_0\omega}\frac{\partial\xi}{\partial z} A^2 = -\frac{1}{2\mu_0\omega}\left\{F_R\frac{dF_I}{dz} - F_I\frac{dF_R}{dz}\right\}. \tag{7}$$

The coupled equation set, Equations (3–6), is integrated in z by specifying the boundary conditions on the profile function $F(z)$ at the entrance ($z = 0$) and

the exit ($z = L$) of the cavity and the initial condition on the beam at the entrance of the cavity. These conditions will depend on the mode of operation of the device. For self-oscillation in a single cavity, the initial states of the electron are chosen to model the injection of a monoenergetic beam with uniform distribution in phase and cross section. Axial velocity spread is introduced through a Gaussian pitch angle distribution. Since an unbunched beam enters the cavity, we assume that the initial amplitude A_0 is zero and the initial phase ξ_0 is arbitrary. We therefore set at $z = 0$,

$$A_0 = 0, \text{ and } \left.\frac{dA}{dz}\right|_{z=0} = b_0 \neq 0 . \tag{8}$$

These conditions represent a conducting wall at $z = 0$. We consider the output end of the cavity to be partially open with a reflection coefficient, R, to model the extraction of power through a window. Hence, at $z = L$, we set the boundary condition

$$\left.\frac{dF}{dz}\right|_{z=L} = i\,k_z(L)\,\frac{1+R}{1-R}\,F(L) \qquad (R \neq 1) , \tag{9}$$

where $k_z(L) = \sqrt{\omega^2/c^2 - k_t^2}$ and k_t is the transverse wave vector of the output section. For fixed beam parameters, cavity parameters, and magnetic field, the initial conditions on the RF field are completely specified by the initial derivative of the profile function b_0 and the oscillation frequency ω. Solutions to Equations (3–6) exist for discrete pairs of values of b_0 and ω, which represent the eigenmodes and eigenvalues of the self-excitations. Since F is complex, Equation (9) constitutes two conditions, and the two parameters, b_0 and ω, are determined by a two-dimensional Newton-Raphson search procedure. The iterative process is started with initial guesses for b_0 and ω, integration of Equations (3–6) is carried out by 4th order Runge-Kutta method, and the values of the two parameters are updated by testing the two conditions in Equation (9). The iterations are continued until Equation (9) is satisfied.

The initial conditions of the particles and the boundary conditions on $F(z)$ for multi-cavity gyroklystron amplifier configuration are different from the above. The beam power is to be maintained below the threshold level of self-excitation in all cavities. When a signal is applied to the input cavity, all cavities oscillate at the impressed frequency. The initial condition on the beam at the entrance of the input cavity is the same as in the single cavity discussed above, but the phase-space distribution of the particles at the entrance of all subsequent cavities is determined by the modulation produced in previous stages. The choice of boundary conditions for the RF field at each stage of the amplifier is more complicated. The drift region between cavities is supposed to be cut off to RF fields. We assume that the signal is side-coupled to the input cavity and choose a sinusoidal field profile having a maximum amplitude consistent with the input power. The field profile is determined self-consistently in other bunching cavities and the power extraction cavity. In the gyroklystron amplifier configuration, the oscillation frequency in each cavity is fixed by the input signal, and the eigenmodes of the cavity are determined by the initial phase and amplitude. Since a bunched beam enters the bunching and output cavities, the initial phases (ξ_{oi}) are not arbitrary and the initial amplitudes (A_{oi}) are nonzero. At the exit of each bunching

cavity we apply the boundary condition $F = 0$ since the RF is cut-off in the drift tubes. The condition of Equation (9) is applied at the exit of the output cavity. The iterative search procedure to satisfy the boundary conditions is performed with the two variables A_{oi} and ξ_{oi} or the complex variable $F_{oi}(i = 2, 3, \ldots, n$ where n is the number of cavities). A simpler one-dimensional root finder for complex functions can be used for this configuration.

The search procedure has to be applied successively to all cavities and becomes time-consuming for a configuration with more than two cavities. For such cases, we adopt a simpler approach based on the assumption that the small-signal condition holds for all cavities except the output cavity. A self-consistent small-signal analytical theory[11] for the multi-cavity gyroklystron developed previously is used to calculate the modulation of the beam produced by the bunching cavities and the input power required in the first cavity. The search procedure to determine the eigenmodes is therefore necessary only in the ultimate cavity. The calculated distribution of particles in momentum and space at the end of the bunching regions serves as input for the large-signal analysis in the ultimate cavity to obtain the overall efficiency and gain of the device. For perfect input coupler, the signal power in the first cavity is given by $P_{in} = \frac{\omega U}{Q_1} - \eta_1 P_b$, where P_b is the beam power, η_1 the efficiency in the first cavity, Q_1 the quality factor, and U the stored energy in TE_{101} mode. If the coupling is not perfect, P_{in} is modified to account for the coupling loss. For gyroklystron amplifier operation, the operating conditions in the input cavity is selected to make η_1 slightly negative to ensure the suppression of self-excitations. In any case, η_1 should not exceed $\omega U/Q_1 P_b$.

4 EXPERIMENTAL RESULTS

Starting at the previous[6] electron gun voltage of 35 kV, this voltage was gradually increased and α was adjusted for optimum amplifier performance at each new value of voltage. Steady improvement in amplifier performance was realized until a gun voltage of approximately 45 kV was reached. For larger voltages, performance rapidly deteriorated due to the electron beam interception at higher α. Numerical simulation of the electron trajectories indicated that there was significant interception of electrons by the walls of the beam tunnel between the electron gun and the input cavity when voltage exceeded about 45 kV.

The detailed process of optimization of gyroklystron performance by adjusting the magnetic field and tuning the penultimate cavity has been published.[6] The magnetic field shown in Figure 2, along with the penultimate cavity tuning provides the optimum beam bunching through the maximum capacitive loading in the penultimate cavity. The efficiency of the three-cavity gyroklystron depends strongly on the magnetic-field profile. Beam loading of the gyroklystron cavities has been observed to be strongly dependent on the magnetic field value.[12] Magnetic tuning is employed, therefore, in the present experiment to shift the hot resonant frequency of the penultimate cavity down for optimum bunching. The magnetic field is tapered down along the output cavity to maintain resonance during energy extraction to maximize the efficiency.

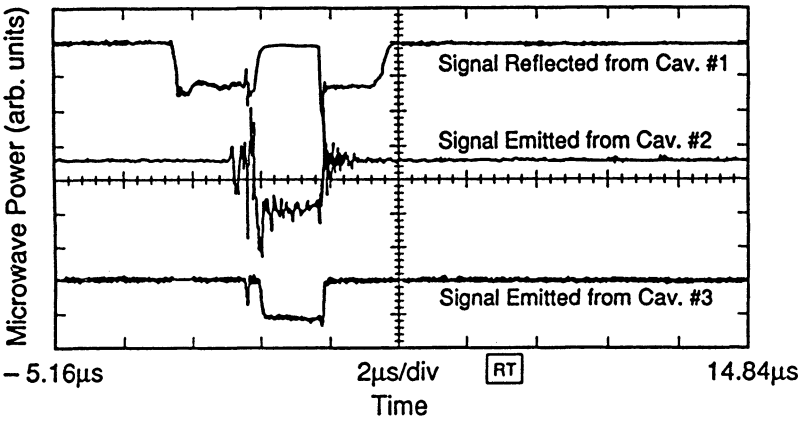

FIGURE 3: Recordings of microwave signals reflected from cavity 1, and emitted from cavities 2 and 3.

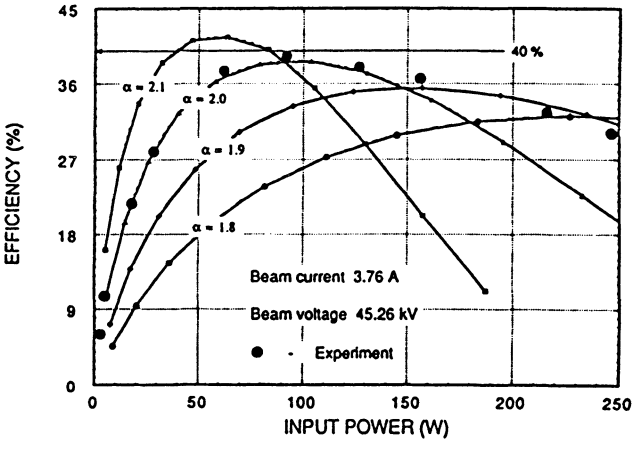

FIGURE 4: Calculated gyroklystron efficiency vs. RF input power and experimental data.

The microwave drive signal coupled into cavity 1 had a pulse width of 3 μs, while the time duration of the electron beam pulse was 1 μs. In Figure 3, typical recordings of the microwave signals reflected from cavity 1 and emitted from cavities 2 and 3 are shown. It may be seen that when the 1-μs. electron pulse passes through cavity 1, effectively all the input microwave power is absorbed by the beam and amplified microwave pulses appear in cavities 2 and 3.

Efficiency of the amplifier vs. input power at an optimum gun voltage of 45.3 kV is shown in Figure 4. A family of theoretical curves is shown for various values of

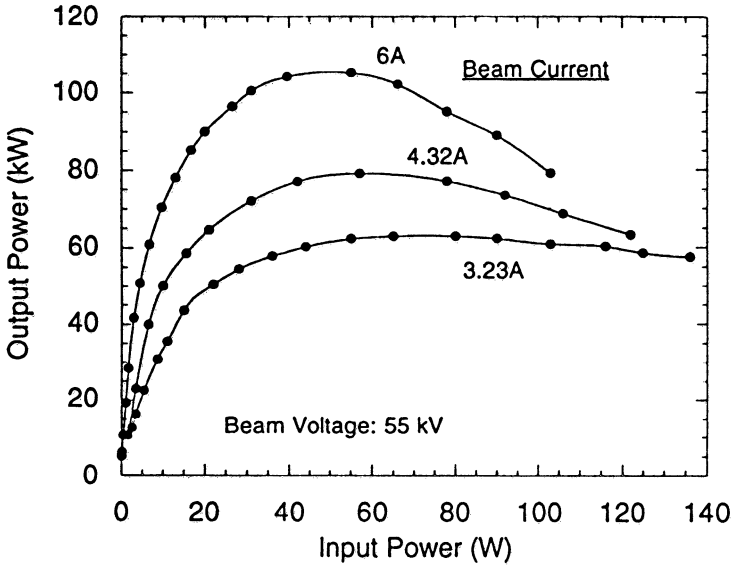

FIGURE 5(a): Output power vs. input power for the three-cavity gyroklystron.

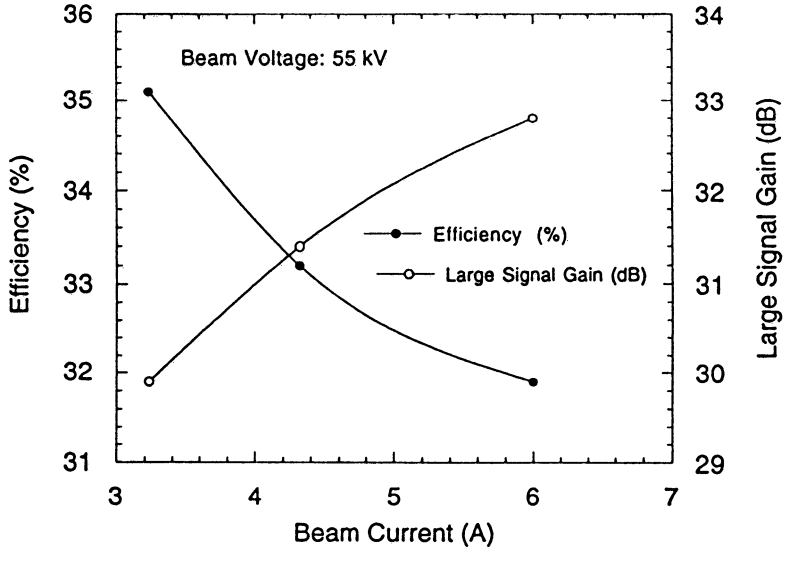

FIGURE 5(b): Efficiency and large signal gain vs. beam current for the three-cavity gyroklystron.

TABLE 1: Gyroklystron experiment parameters

	Experiments			
	Bollen *et al.*, 1985	Park *et al.*, 1992	This Work	
Voltage (kV)	35	33	45	55
Current (A)	7.5	4	3.8	6
Beam α (estimated at entrance to cavity #1	1	1.8	2	< 1.5
Efficiency (%)	21*	30	40	32
Saturation Gain (dB)	18	30	30	32
Output Power (kW)	52	37	68	105

* Efficiency of 33% was reported with reduced output power.

pitch angle, α. The small signal gain is higher at larger values of α, and therefore the input power for peak efficiency decreases with increasing α. Also, since for the most part transverse electron energy alone is converted to microwave radiation in the output cavity, the peak efficiency is enhanced as α becomes larger.

Also shown in Figure 4 are the experimentally measured data points at the optimum voltage of 45.3 kV. Agreement between the experimental points and the theoretical curve for $\alpha = 2$ is excellent for input powers of up to 150 watts. Peak output efficiency is seen to be almost 40% when the input power is 70 watts; the corresponding output power is 68 kW, so the saturated gain is $\sim$30 dB.

Results for operation at the higher beam voltage of 55 kV are shown in Figures 5a and 5b. The experiment was carried out with a beam which was unoptimized due to electron interception at the end of the gun region. Under these circumstances the beam α was approximately 1.5. The beam current was varied, and changes in the output power, efficiency, and gain were noted. As shown in Figure 5a, for a beam current of 6 A, more than 100 kW of output power has been obtained at a beam voltage of 55 kV. When the beam current was increased, the device gain increased and the efficiency decreased as expected.

In Table 1 the optimum power and efficiency point is tabulated. It is compared in the table with previous experiments at $\sim$ 35 kV.[6, 13] The experiment of Bollen *et al.*[13] achieved an output power of 52 kW and a corresponding efficiency of 21%, with a tapered magnetic field. Bollen *et al.* also reported achieving efficiency as large as 33% with a reduced beam current, and corresponding output power was significantly smaller. In the experiment of Park *et al.*,[6] performance was optimized both by shaping the magnetic field and by detuning the penultimate cavity; output power was 37 kW with a corresponding efficiency of 30%. Note especially that increasing the operating voltage to 45 kV in the present experiment increased not only output power but also efficiency.

5 DISCUSSION

The three-cavity gyroklystron operating at 45 kV has shown the highest operating efficiency to date (viz. 40%) for any gyroklystron with output power $\gg$ 1 kW. At the 40% efficiency point, saturated gain was 30 dB and output power was 68 kW. Agreement of the experimental data with theoretical predictions is excellent for pitch angle in the range $1.9 < \alpha < 2.0$. Thus transverse efficiency was about 50%.

It is remarkable that the original design efficiency[5] of 40% was achieved even though the gyroklystron was still operated at a derated voltage (45 kV, compared to the design value of 60 kV). This is attributable to the omission of the effects of magnetic-field tapering and penultimate cavity detuning from the original design. It is anticipated that when a gyroklystron with large pitch angle (i.e. $\alpha \sim 2$) is operated at its full design voltage in an optimized way, an operating efficiency significantly above the present 40% will be realized.

Finally, we take this opportunity to point out that although amplifier noise was not measured in the present experiment, a previous noise study[14] did indicate that the gyroklystron signal is of sufficient quality to be useful for large linear accelerators. With a three cavity TE_{101}-mode gyroklystron similar to the one in the present experiment, driven by a 30 kV, 5 A, $\alpha = 1.5$ electron beam, the phase fluctuation was 4.2° per 1% fluctuation in beam voltage.[14] With an amplifier voltage of 400–500 kV, the phase fluctuation is predicted14 to be several times larger, but can likely be reduced to acceptable levels by feedback techniques.

REFERENCES

1. R.S. Symons and H.R. Jory, "Cyclotron Resonance Devices," in *Advances in Electronics and Electron Physics*, vol. 1 (Academic Press, New York, 1979), pp. 1–54.
2. S. Tantawi *et al.*, "High-power X-band amplification from an overmoded three-cavity gyroklystron with a tunable penultimate cavity," IEEE Trans. Plasma Sci. **20** (1992), p. 205.
3. W. Lawson *et al.*, "High power operation of a K-band second harmonic gyroklystron," Phys. Rev. Lett. **71** (1993), p. 456.
4. R.D. Ruth, "Progress on Next Generation Linear Colliders," AIP Conference Proceedings **184**, M. Month and M. Dienes, editors American Institute of Physics, (1989), pp. 2209–2226.
5. B. Arfin and A.K. Ganguly, "A three-cavity gyroklystron amplifier experiment," Int. J. Electron. **53** (1982), p. 709.
6. G.S. Park *et al.*, "Experimental study of efficiency optimization in a three-cavity gyroklystron amplifier," IEEE Trans. Plasma Sci. **20** (1992), p. 224.
7. A.K. Ganguly and S. Ahn, "Self-consistent large signal theory of the gyrotron traveling wave amplifier," Int. J. Electronics **53** (1982), p. 641.
8. A.K. Ganguly and S. Ahn, "Nonlinear theory of the slow-wave cyclotron amplifier," Phys. Rev. A **42** (1990), p. 3544.
9. A.K. Ganguly and S. Ahn, "Nonlinear analysis of the gyro-BWO in three dimensions," Int. J. Electron. **67** (1989), p. 261.
10. A.K. Ganguly *et al.*, "Three dimensional nonlinear theory of the gyropeniotron amplifier," Int. J. Electron. **65** (1988), p. 597.
11. A.K. Ganguly *et al.*, "Theory of multicavity gyroklystron amplifier based on a green's function approach," IEEE Trans. Plasma Sci. **13** (1985), p. 409.

12. G.S. Park *et al.*, "Passive gyrotron cavity loading and frequency shift," Int. J. Electronics **72** (1992), p. 921.
13. W.M. Bollen *et al.*, "Design and performance of a three-cavity gyroklystron amplifier," IEEE Trans. Nucl. Sci. **32** (1985), p. 2879.
14. G.S. Park *et al.*, "Phase stability of gyroklystron amplifier," IEEE Trans. Plasma Sci. **19** (1991), p. 632.